A Lanczos transformation for impurity problems on a lattice: Dimensionality and boundary effects

C. A. Büsser,[1] G. B. Martins,[2] and A. E. Feiguin[3]

[1]*Department of Physics and Arnold Sommerfeld Center for Theoretical Physics, Ludwig-Maximilians-University Munich, Germany**
[2]*Department of Physics, Oakland University, Rochester, MI 48309, USA*
[3]*Department of Physics, Northeastern University, Boston, Massachusetts 02115, USA*

We present a completely ambiased and controlled numerical method to solve quantum impurity problems in *d*-dimensional lattices. This approach is based on a canonical transformation, of the Lanczos form, where the complete lattice Hamiltonian is exactly mapped onto an equivalent one dimensional system, in the same spirit as Wilson's Numerical Renormalization. The method is particularly suited to study systems that are inhomogeneous, and/or have a boundary. As a proof of concept, we use the density matrix renormalization group to solve the equivalent one-dimensional problem. The resulting dimensional reduction translates into a reduction of the scaling of the entanglement entropy by a factor L^{d-1}, where L is the linear dimension in the original d-dimensional lattice. This allows one to calculate the ground state of a magnetic impurity embedded into an $L \times L$ square lattice and an $L \times L \times L$ cubic lattice with L up to 140 sites. We also study the localized edge states in graphene nanoribbons by attaching a magnetic impurity to the edge or the center of the system. For armchair metallic nanoribbons we find a slow decay of the spin correlations as a consequence of the delocalized metallic states. In the case of zigzag ribbons, the decay of the spin correlations depends on the position of the impurity. If the impurity is situated in the bulk of the ribbon, the decay is slow as in the metallic case. On the other hand, if the adatom is attached to the edge, the decay is fast, within few sites of the impurity, as a consequence of the localized edge states, and the short correlation length. The mapping can be combined with ab-initio band structure calculations to do a realistic modeling of the system, and to understand correlations effects in quantum impurity problems from first principles.

PACS numbers: 73.23.Hk, 72.15.Qm, 73.63.Kv

I. INTRODUCTION

The Kondo problem describes a magnetic impurity embedded in a Fermi sea[1,2]. The spin of the impurity is screened by the spins of the electrons in the bulk forming a collective singlet state. Even though this is one of the most studied and better understood problems in condensed matter physics, we keep finding that our knowledge is incomplete, and open issues remain. In particular, there are questions that require a good description of the states and correlations in real space. For instance, great attention has been payed to the subtle issues of how to measure, detect, and characterize the so-called "Kondo cloud"[3–6], or how to interpret the finite-size effects and competing energy scales arising when the conduction electrons are confined to small spatial region in a "Kondo box"[7–11]. Moreover, systems where the spatial position of the impurity is relevant (such as graphene nanoribbons, or topological insulators, where the physics of the edges is very different than the physics of the bulk) are quite non-trivial and represent a challenge to current state-of-the-art methods.

In the most general formulation of the problem the interactions between the impurity and the lattice will have terms of the form $V_k d_\sigma^\dagger c_{k\sigma} \exp(-ir_0 k)$ (where r_0 is the position of the impurity and we used the normal notation thus $d_\sigma^\dagger$ create an electron at the impurity site with spin σ and $c_{k\sigma}$ destroy an electron with spin σ at the k state). One of the usual approximations is to take simple forms for the dispersion ϵ_k or to ignore the momentum dependence of the couplings V_k, disregarding the information about the specific structure of the lattice[12–15]. Most commonly, one finds the impurity interacting with a wide band with a linear dispertion, via a contact local potential. This corresponds to the impurity being scattered only by s-wave states, and the problem can be mapped to an equivalent one-dimensional one.

Systems where the effect of energy psudogaps or Van-Hove singularities are important represent a challenge, and it is known, for instance, that the Kondo effect in graphene is quite non-trivial[16–21]. Moreover, approximations on the couplings V_k make it difficult to deal with problems where the location of the impurity is relevant. As an example of this later situation we can mention graphene nanoribbons, or topological insulators, where the physics of the surface/edges is very different than the physics of the bulk. At the same time, experiments with adatoms on surfaces can be done with great degree of control using techniques such as STM[22–29] , and methods that can deal with the spatial resolution of the Kondo problem are very important.

Numerical Renormalization Group (NRG), the optimal technique to study quantum impurities, does not work in a real space representation, but in energy space[12,15]. Until recently, Quantum Monte Carlo (QMC) was the only computational technique that could offer some detail on the spatial structure of the correlations in dimensions larger than $d = 1$[30–34]. Very recently, remarkable developments in the understanding of the NRG construction and its wave functions have offered a glimpse at the spatial structure of correlations around the impurity[35–37]. Moreover, using some ingenuity it is possible to introduce arbitrary dispersion/densities of states for the conduction electrons[38,39].

In this work, we introduce a new computational approach that enables one to work with the lattice in a real space representation at arbitrary dimensions with the density matrix renormalization group(DMRG)[40–43]. The principal idea is to map, via a canonical transformation, the lattice onto a

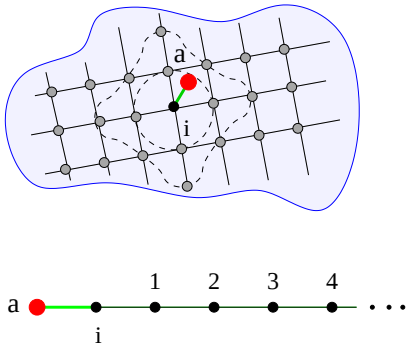

FIG. 1: *Mapping of the system into a semi-chain*. Using the Lanczos method a real lattice can be mapped into a 1d semi-chain. The coupling between the impurity and the real lattice, shown in panel (a), determine the construction of Lanczos seed $|\Psi_0\rangle$. In this case the seed is given just for a single site i that become the first site of the mapped chain, shown in panel (b).

chain structure, in similar fashion as Wilson's original NRG formulation[12]. However, in our formulation the lattice structure and the coupling will be completely preserved. Notice that this canonical transformation is exact, and the new representation of the Hamiltonian can be tackled with other methods especially suitable for solving the one-dimensional problem such as the embedded cluster approximation (ECA)[6], or the DMRG.

II. MAPPING BANDS ONTO CHAINS

Let us start with a simple Hamiltonian with one impurity connected to one single lattice site. A more general case will be discussed below. The Hamiltonian is

$$H = H_{\rm imp} + H_{\rm band} + V, \tag{1}$$

where $H_{\rm imp}$ is the many body impurity Hamiltonian, $H_{\rm band}$ is the Hamiltonian for the lattice and V describes the interaction between the impurity and the lattice. For the Anderson model, the impurity is described by

$$H_{\rm imp} = V_g \sum_\sigma n_{d\sigma} + U n_{d\uparrow} n_{d\downarrow}, \tag{2}$$

where $n_{d\sigma}$ is the occupation operator for the impurity with spin σ, V_g is a gate potential, and U parametrizes the on-site Coulomb repulsion between electrons.

The corresponding hybridization term is introduced as

$$V = t' \sum_\sigma d^\dagger_\sigma c_{{\rm r}_0\sigma} + {\rm h.c.}, \tag{3}$$

where $d^\dagger_\sigma$ creates an electron at the impurity and $c_{{\rm r}_0\sigma}$ destroys an electron at the lattice site connected to the impurity, at ${\rm r}_0$.

Alternatively, one could introduce the impurity via a Kondo Hamiltonian, with an interaction

$$V = J_K \vec{S}_d \cdot \vec{S}_{{\rm r}_0} \tag{4}$$

The main point of this proposal is to map a complex band structure, for example a carbon nanotube, a graphene ribbon, or any 2d or 3d system, onto a semi-chain. This mapping can be done in such a way that an impurity connected to one or more sites of the a real lattice is, after the mapping, connected to a single site of a chain. The resulting one-dimensional system can then be solved with a method of choice, such as ECA or DMRG.

In order to perform the mapping, we need to assume that the band describes non-interacting electrons via a quadratic tight-binding Hamiltonian. One can always map a complicated one body Hamiltonian onto a semi-chain by applying the Lanczos method in the same spirit as Wilson's NRG[44]. To start the change of basis, we choose the orbital that is connected to the impurity as seed for the iterative procedure[45]:

$$|\Psi_0\rangle = c^\dagger_{{\rm r}_0}|0\rangle. \tag{5}$$

The so-called Lanczos basis is constructed as:

$$|\Psi_1\rangle = H_{\rm band}|\Psi_0\rangle - a_0\,|\Psi_0\rangle \tag{6}$$
$$|\Psi_{i+1}\rangle = H_{\rm band}|\Psi_i\rangle - a_i|\Psi_i\rangle - b_i^2|\Psi_{i-1}\rangle. \tag{7}$$

where,

$$a_i = \frac{\langle\Psi_i|H_{\rm band}|\Psi_i\rangle}{\langle\Psi_i|\Psi_i\rangle}, \qquad b_i^2 = \frac{\langle\Psi_i|\Psi_i\rangle}{\langle\Psi_{i-1}|\Psi_{i-1}\rangle}.. \tag{8}$$

This allows one to construct a basis where the lattice Hamiltonian $H_{\rm band}$ is tri-diagonal.

$$H_{\rm band} = \begin{pmatrix} a_0 & b_1 & 0 & 0 & \cdots \\ b_1 & a_1 & b_2 & 0 & \cdots \\ 0 & b_2 & a_2 & b_3 & \cdots \\ 0 & 0 & b_3 & a_3 & \cdots \\ \vdots & \vdots & \vdots & \vdots & \end{pmatrix} \tag{9}$$

This is an exact canonical transformation, from a single particle basis, onto another complete orthogonal basis.

In Fig.1(a) we show a schematic representation of the total Hamiltonian in real space. Panel (b) shows the same Hamiltonian in the Lanczos basis. The off-diagonal matrix elements become effective hopping terms, while the diagonal ones introduce local chemical potentials. In second quantization, it reads:

$$H_{\rm band} = \sum_{i=0}^{N} a_i \tilde{n}_i + \sum_{i=0}^{N-1} b_{i+1} \left(\tilde{c}^\dagger_{i\sigma} \tilde{c}_{i+1,\sigma} + {\rm h.c.} \right), \tag{10}$$

where the new "tilde" operators refer to the Lanczos orbitals along the chain. Notice that the first orbital, corresponding to the one connected to the impurity and used as seed, remains unaltered after the transformation, *i.e*, $\tilde{c}_0 \equiv c_0$. As a consequence, the Hamiltonian V remains invariant.

In the process of generating the new basis we find that:

1. $\langle\Psi_j|\Psi_i\rangle = \delta_{i,j}$

2. $\langle\Psi_j|H_{\text{band}}|\Psi_i\rangle = b_i\delta_{j,i+1} + a_i\delta_{i,j}$

3. The basis $\{|\Psi_n\rangle\}$ is orthogonal but it is not normalized.

4. Obviously, once one of the b_n vanishes, the rest of the band will decouple. In fact, all $|\Psi_m\rangle$, for $m > n$, will not be defined (the rest of the basis belongs to different channels/symmetry sectors).

5. As $\langle\Psi_n|\Psi_n\rangle$ grows with n, numerical errors due to finite numerical precision might appear. To avoid them, we have to re-normalize the states $|\Psi_{i-1}\rangle$ at each iteration.

6. Another numerical error to consider is the loss of orthogonality between vectors for large n. To avoid that, and keep the basis complete, we orthogonalize each new vector with all the previous vectors in each iteration.

The transformation can also be applied to problems where either the band, or the impurity, have a more complex structure, as described in the following sections.

III. GEOMETRICAL INTERPRETATION AND ENTANGLEMENT

The structure of the Lanczos orbitals can be intepreted geometrically in a very simple way, for a system such as the square lattice. The reference site where the impurity is attached becomes a center of symmetry for the point group operations of the lattice, as shown in Fig.1. Since the hoping Hamiltonian obeys the same symmetries, the Lanczos orbitals will belong to the same symmetry sector as the seed orbital. If the impurity is attached locally to a single site of the lattice, all the orbitals will have "s-wave" symmetry, invariant under rotations of the lattice with all positive coefficients. This corresponds to the trivial representation of the point group of the lattice. All other channels, corresponding to different symmetry classes, will form their own independent chains, and will be completely decoupled from the impurity. This yields a remarkable result: in order to study a system with L^d sites (where L is the linear size, and d the dimensionality of the problem), we only need to keep $N \sim \mathcal{O}(L)$ orbitals!

The orbitals are then defined by their symmetry sector, and their radial distance from the center of symmetry, which is correlated to the linear distance along the equivalent 1d chain. Notice that in a bipartite lattice, odd and even sites along the chain will correspond to orbitals with support on different sublattices, a result that will become important in the interpretation of numerical results.

As a consequence of these observations, we obtain an intuitive understanding of the behavior of the entanglement: The entanglement *per channel* between the region enclosed by an area of "radius" L in the d-dimensional problem is exactly the same as the entanglement between the first L sites of the chain, and the rest. Since the chain is a critical one-dimensional system (for square and cubic lattices, for instance), the von Neumann entanglement entropy is proportional to $\log(L)$[46,47]. All chanels contribute to the entropy with similar factors. It can be seen that the number of chanels is proportional to the area of the boundary $\sim L^{d-1}$. This yields a final result proportional to $L^{d-1}\log(L)$. Therefore, based on these simple arguments, we can easily understand why free fermions in higher-dimensions have logarithmic corrections to the area law[48–51]. The advantage of our approach is that we only need to solve the problem in the trivial channel that is coupled to the impurity, reducing the entanglement by a factor of L^{d-1}!.

Notice that these ideas are basically a generalization of the one dimensional case studied in Ref.52. In a one dimensional impurity problem, one can apply reflection symmetry and make a "folding" transformation, mapping the single particle orbitals onto bonding and antibonding states. In that case, the impurity couples only to the bonding channel, while the anti-bonding remains decoupled. This translates into a reduction of the entanglement by a factor of 2.

We point out that in generic situations, the coupling between the impurity and the lattice could be along a different channel in a different symmetry sector. Moreover, it could couple to more than one channel at the same time. Tackling this problem is explained in the next section.

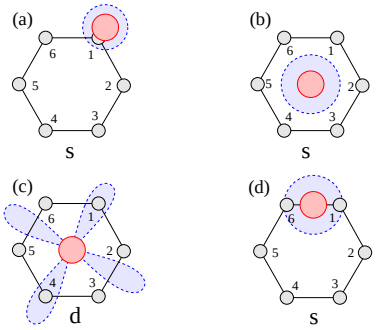

FIG. 2: *Choosing the seed.* Examples of how the coupling between the impurity and the lattice will determine the construction of the seed. We are using an honeycomb lattice but the idea can be extended to any lattice. (a) The simplest case (and the one used for the calculations in the rest of the paper), the impurity is sitting on top of just one atom. (b) The impurity is connected to all six sites. (c) The impurity is has an orientation dependent hybridization with the lattice. (d) The impurity is on the bond between two C atoms.

IV. CONSTRUCTING THE SEED ORBITAL

As discussed above one of the central issues in the canonical transformation is how to pick the right seed $|\Psi_0\rangle$. This is determined by the chemistry of the problem and several situations can arise. In the simplest scenario, the impurity can be connected to a single site, but in the general case they can interact with several orbitals of the lattice. In Fig. 2, as an illustration, we show the case of one adatom in an honeycomb

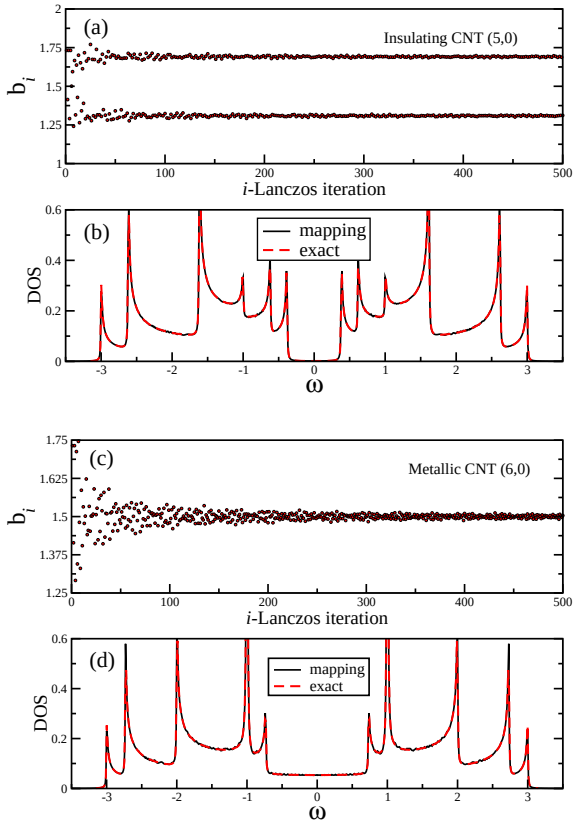

FIG. 3: *Local density of states for CNT and hopping parameters for a single chain mapping.* The LDOS as function of ω and chain hopping vs. n are shown for an insulating (top) and a metallic (bottom) CNT. For the LDOS the exact solution calculated using Green functions is shown in red dashed lines.

lattice. The adatom can sit on top of one of the atoms of the lattice (a) or in the middle of an hexagon (b). Depending on the hybridization with the lattice, it can couple symmetrically to all six sites or have anisotropic couplings, as shown in panel (c). Finally, the impurity can be connected along the bond between two carbon atoms (d). The general form for the coupling Hamiltonian for the impurity will be of the form

$$V = \sum_{i=1..6\ \sigma} t_{0i}\ d^\dagger_\sigma\ c_{r_i\sigma} + \text{ h.c.}, \tag{11}$$

Then, we define an orbital

$$c_{r_0\sigma} = \sum_i \frac{t_{0i}}{\tilde{t}_0}\ c_{r_i\sigma}, \tag{12}$$

and re-write the Hamiltonian as:

$$V = \sum_\sigma \tilde{t}_0\ d^\dagger_\sigma\ c_{r_0\sigma} + \text{ h.c.}, \tag{13}$$

where we have used the definition $\tilde{t}_0 = \sqrt{\sum_i t^2_{0i}}$. Now, the seed can be defined as,

$$|\Psi_0\rangle = c^\dagger_{r_0}|0\rangle. \tag{14}$$

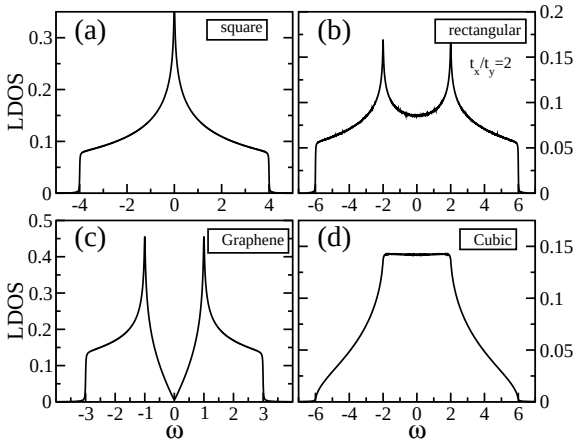

FIG. 4: *LDOS for several lattices.* The Local Density of States is plot as function of ω for a 2d square lattice with 800^2 sites (a), a rectangular lattice with 800^2 sites (b), graphene with 800^2 sites (c) and a 3d cubic lattice of 200^3 sites.

Notice that this is possible because the coupling Hamiltonian has only one body terms, such as the case of Anderson-type Hamiltonians. For coupling Hamiltonians that contain many-body terms, if the impurity is connected to more than one site, it is not possible to chose such a simple seed. In that case, the proper way to identify the coupling Hamiltonian is by a Schrieffer-Wolff transformation. The seed to use in that case can be obtained by a generalization of these ideas.

V. NON-INTERACTING RESULTS

As a first benchmark test we present the calculation of one body properties for a system without impurities. We compare the local density of states (LDOS) obtained at the position of the seed orbital which is not changed by the basis transformation. Since this is a single body problem, exact results are known.

We start by calculating the mapping for carbon nanotubes (CNT). As it is well known, depending of the direction of grow, or chirality, a CNT can be metallic or insulator[53]. In Figure 3 we present results for the hopping parameters in the mapped chain and the LDOS. We analyze two different types, one being insulating and the other metallic.

In panels (a) and (b) we present the insulating case, which displays gap at the middle of the LDOS. We observe twelve Van Hove singularities, indicating a complex band structure. We compare the result with those obtained by direct diagonalization, shown in the figure with red-dashed lines. No difference between them can be appreciated.

The hopping parameters for the resulting chain are shown in panel (a), and we observe two families of hoppings/energy scales, around $t_a \sim 1.7$ and $t_b \sim 1.3$. This repeated structure (A-B-A-B-A-B-A-B...) resembles a superlattice with a two-site basis (A-B). As a consequence, the band structure develops a gap. Of course there are other lower frequency structures in the hopping elements associated to the six Van

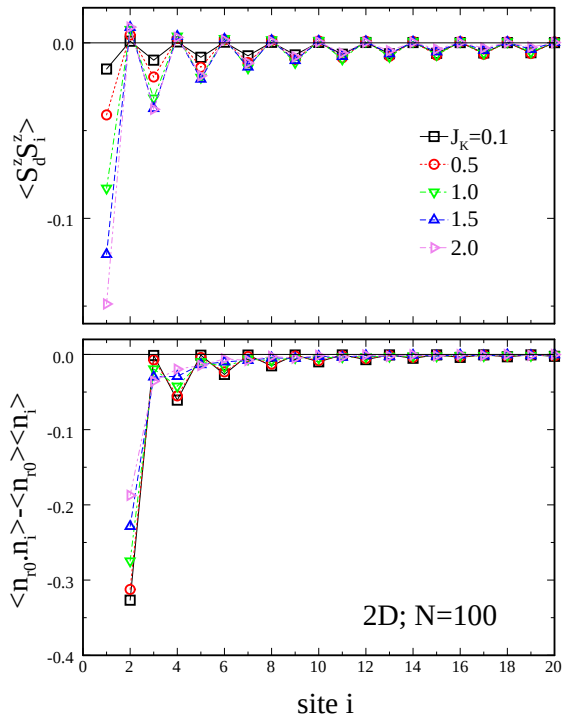

FIG. 5: *Correlations for a 2d square lattice.* (a) Spin-spin correlations between a Kondo impurity and the rest of the chain, for different values of J_K, and keeping $N = 100$ sites. We show results for the first 20 sites of the chain. (b) density-density correlations between the first site of the chain, and the rest. All simulation are at half-filling. Notice that this system size corresponds to an actual square lattice with $N \sim 140^2$ sites.

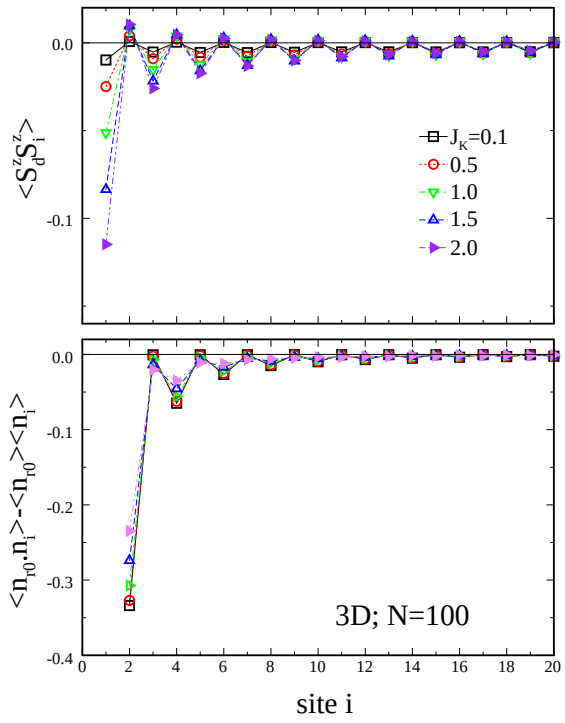

FIG. 6: *Correlations for a 3d cubic lattice.* (a) Spin-spin correlations between a Kondo impurity and the rest of the chain, for different values of J_K, and keeping $N = 100$ sites. Same as before, we show results for the first 20 sites of the chain. (b) density-density correlations between the first site of the chain, and the rest. Notice that this system size corresponds to an actual cubic lattice with a diagonal size of 100 sites.

Hove singularities inside each band.

In panels (c) and (d) of Fig. 3 we show results for the metallic CNT. In this case we can see ten Van Hove singularities in the LDOS. Again, we compare with the exact solution and the agreement is excellent. For the hopping parameters in the chain we do not have, this time, the dimer structure that we observed in the previous case.

For illustration we also present results for higher-dimensional systems. As expected, we reproduce exactly all the features of the spectrum, such as the Van Hove singularity at $\omega = 0$ for the 2d square lattice, shown in Fig. 4(a). In the case of a rectangular lattice, where the lattice parameter in one direction is twice the other, we see that the Van Hove singularity is split in two peaks, shown in Fig. 4(b). The 3d density of state provides is a nice simple testbed to study the problem with a quasi-flat DOS, such as the one used in analytical treatments of the Kondo model, and its Bethe Ansatz solution. We can also reproduce, after the mapping, the band structure of graphene, where we recover the massless Dirac modes at $\omega = 0$. Needless to say, these results are not surprising, since the proposed mapping is an exact canonical transformation.

VI. DMRG SOLUTION OF THE EFFECTIVE 1D PROBLEM

In order to study the many-body problem with an interacting impurity, we use the DMRG method, which is specially suitable for one-dimensional problems. We perform the mapping for the band Hamiltonian and we solve the full problem, with the impurity connected to the first orbital of the chain, which also served as the seed to construct the Lanczos basis. Obtaining the mapping for large systems is straightforward, but in order to do a DMRG calculation we limit the sizes to a few hundred sites, and we perform a finite size scaling in $1/N$, where N is the linear dimension of the problem, as displayed in Fig.7a. In all calculations we kept the DMRG truncation error below 10^{-9}.

As a proof of concept we solve the Kondo Hamiltonian (4) first. In Fig.5(a) we show the spin-spin correlations between the impurity and the Lanczos orbitals of the chain $\langle S_d^z S_i^z \rangle$ as a function of the distance from the impurity, and the value of J_K. We see a characteristic power-law behavior, with alternating antiferromagnetic (AFM) and ferromagnetic sign. The ferromagnetic correlations within the same sublattice increase with J_K. The density-density correlations are plotted in panel (b). In this case we show the correlations between the first site of the chain and the rest $\langle n_{r_0} n_i \rangle - \langle n_{r_0} \rangle \langle n_i \rangle$. In Fig.6

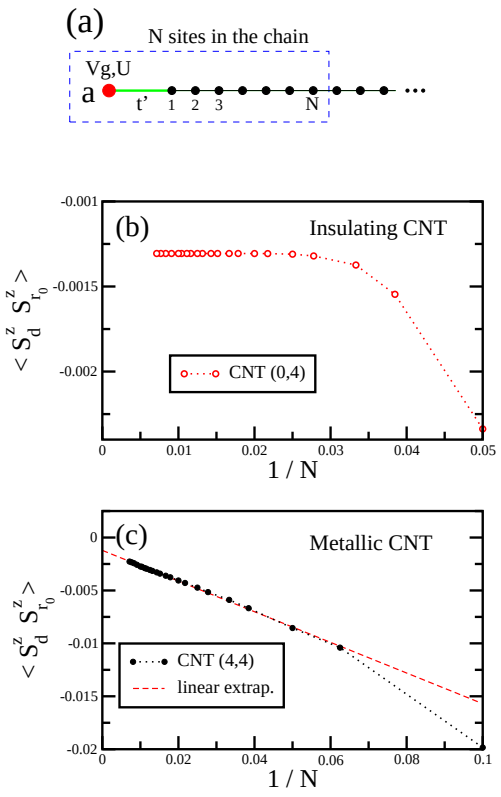

FIG. 7: *Scaling of correlations in CNTs using DMRG.* (a) In order to extrapolate to the thermodynamic limit we first we map the band Hamiltonian onto its tridiagonal Lanczos form. We study the convergence as a function of $1/N$, where N is the number of sites kept in the actual simulation. Panels (b) and (c) show the spin-spin correlations as function $1/N$ for an adatom at the surface of a CNT. Panel (b) corresponds to an insulating CNT (0,4). In this case, as there are not extended states in the CNT, and convergence is fast. Panel (c) shows results for a metallic CNT (4,4). Due to the gapless metallic extended states, the convergence is slower. A linear extrapolation in $1/N$ is also shown in the figure. The parameters used here are $U = 1$,$V_g = -U/2$ and $t' = \sqrt{0.05}$.

we show the same quantities for a cubic lattice, which look qualitatively the same. These results reproduce the behavior obtained with other techniques such as QMC[31] and NRG[35]. Notice that the size of the chain corresponds to the radial dimension of the d-dimensional lattice. This means that a chain of length $N = 100$ describes a square or a cube with a half-diagonal of the same size. A detailed study of the correlations will be presented elsewhere.

We next studied the Anderson model (2) for an adatom at the surface of a CNT (all simulations were done at half-filling at the particle-hole symmetric point). In Figs. 7(b) and (c), we show the spin-spin correlations between the impurity and the first orbital $\langle S^z_{\rm d}\ S^z_{\rm r_0}\rangle$ where $\rm r_0$ is the CNT site that is directly connected to the impurity. Results for the CNT(0,4) are shown in the upper panel of Fig. 7. In this case, since the system is gapped, and the correlation length small, we achieve convergence for $N \sim 40$ ($1/N \sim 0.025$). The metallic case for a CNT(4,4) is shown in the lower panel, displaying a linear behavior in $1/N$.

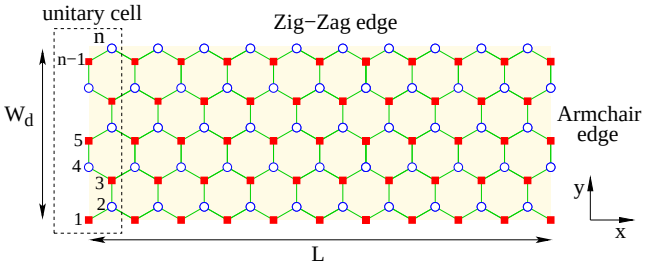

FIG. 8: *Representation of a graphene ribbon.* We show a ribbon with zigzag edges, width W_d and length N. The two triangular sublattices are represented by squares and open circles. The unit cell in the armchair edge direction, containing n sites, is shown in the black-dashed box.

VII. GRAPHENE NANORIBBONS: LOCALIZED VS METALLIC STATES

In the previous section we analyzed two different scenarios with an impurity connected to two and insulating, and metallic nanotube. In this section we apply these ideas to the case of an adatom attached to a graphene nanoribbon.

Since its discovery, graphene[54,55] (a monolayer of graphite with a honeycomb arrangement of carbon atoms) has become the subject of intense research due to its unusual electronic properties, in particular because of its massless Dirac spectrum[56,57]. This makes graphene an ideal experimental system to test for exotic new physics, as well as a promising basis for novel nanoelectronics, raising the expectations for a post-silicon era[58–61] Adding magnetic atoms or defects opens the possibility for spintronic applications, where not only the charge, but also the spin of the electrons can be used in devices[62,63].

The physics of diluted magnetic impurities in 2d graphene is rich and and entire subject of research on its own right[16,64,65]. Isolated magnetic adatoms placed on graphene sheets have been studied experimentally as well as theoretically[56,57], and the properties of the Kondo ground state in graphene has been a subject of controversy. Experimental evidence of Kondo effect due to magnetic adatoms, such as Co, on top graphene has been reported. Depending on the position of the adatom, different behaviors can be observed. For adatoms on top of C sites, a Fermi liquid behavior consistent with a $SU(2)$ Kondo effect has been reported in agreement with the experimental results[66–69] However for adatoms in the center of an hexagon, the results are contradictory. On one side, based on symmetry arguments and DFT calculations, an $SU(4)$ Kondo effect was reported[70,71]. On the other hand, renormalization group arguments show a two-channel Kondo effect with a characteristic non-Fermi liquid behavior[67,72]. Moreover, the Kondo state does not depend only on the position of the adatom, but also on the band filling. By gating graphene, one can more away from the Dirac point to a region of the band with a linear density of states.

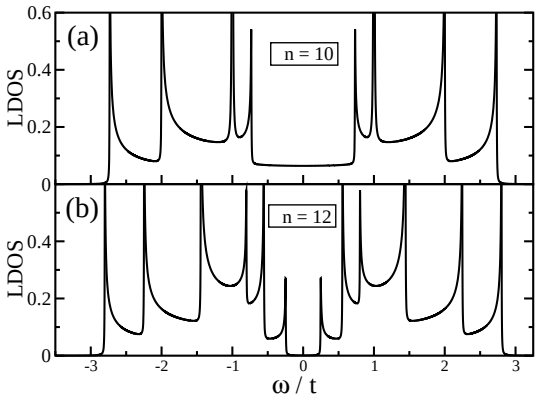

FIG. 9: *Local density of states for armchair ribbons*. The LDOS calculated along the y-direction of the ribbon for a metallic $n = 10$ (a) and insulator $n = 12$ (b) nanoribbons.

In this work we use the nanoribbons just as a proof of concept, and not as an object of study, and we illustrate how the method can be used to identify and study localized edge states.

A. Electronic properties of Graphene ribbons:

Graphene is an arrangement of C atoms in a 2d honeycomb structure, that can be described by two inter penetrating triangular lattices. This is shown in Fig. 8 where a graphene ribbon with zigzag edges is represented. The two sub lattices are presented by squares and open circles.

Is well known that graphene ribbons and carbon nanotubes display similar characteristics. In the case of ribbons, their properties are determined by their edges and widths[73]. Ribbons with zigzag edges are alway metallic with localized edge-states, while armchair ribbons can be insulating or metallic depending on their width. We classify the ribbons by the shape of their longest side (zigzag or armchairs) and by the number of sites n in the unit cell as shown in Fig. 8. We ignore correlation effects, and magnetism, and we focus on the pure electronic properties for the moment. To reconstruct the band structure, we considered a tight-binding Hamiltonian with 7000 unit cells. We use as unit of energy the hopping $t \sim 2.8$eV and for simplicity we neglect the second neighbors hopping $t' \sim 0.1t$[16].

We chose as seeds for the Lanczos process atomic sites at the edge or at the center of the ribbons. Following Ref.69 the adatom is placed on top of a carbon site as shown in Fig. 2(a).

In Fig. 9 we show the total DOS for two different cases of armchair nanoribbons. This LDOS is the average of the LDOS in all the sites of the unit cell of the ribbon. It contains information about both, the edges and bulk states together. The LDOS at each site of the unit cell was calculated after the mapping. In the figure two different armchairs are displayed, one metallic with $n = 10$ sites in the unit cell in panel (a) and the other with $n = 12$ in (b). In this later case the insulating gap is about $0.5t$. Same as for the CNT presented in the previous section the DOS shows a complex structure of Van Hove

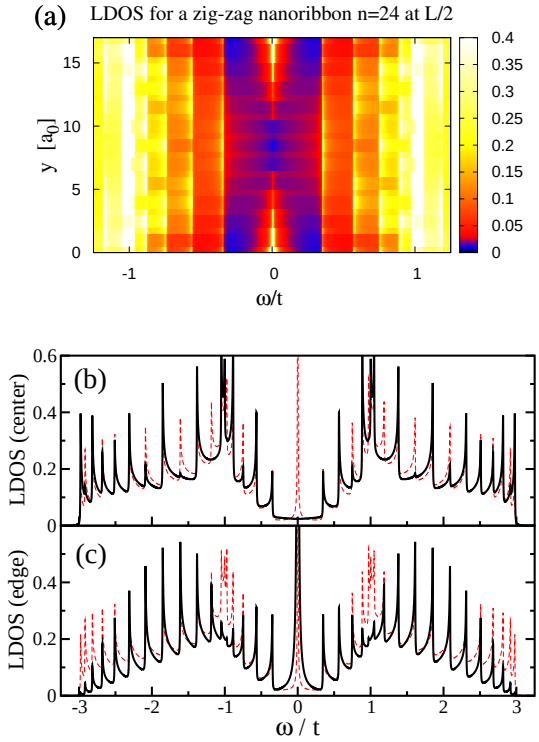

FIG. 10: *Local density of states for zigzag ribbons.* Panel (a) show the LDOS vs ω in the y-direction of a ribbon with $n = 24$ sites in the unit cell. A detail of the LDOS is shown for the center (b) and the edge (c) of the ribbon. In both panels the total DOS, averaged over all sites, is shown in red-dashed lines. A resonance at $\omega = 0$ for the LDOS at the edge is consequence of the localized state. We can see, in panel (a), how this resonance vanishes when we approach the center of the ribbon.

singularities. Increasing the number of sites in the unit cells will increase the number of bands and hence the number of Van Hove singularities.

Figure 10 shows the DOS calculated for a zigzag ribbon with $n = 24$ sites per unit cell. In panel (a) we show the LDOS vs ω and the position inside the ribbon y, around the Fermi energy, $\omega = 0$, for half filling. Panels (b) and (c) present the detail of the LDOS at the edge ($y = 0$) and at the center ($y = 8.75a_0$) of the ribbon. We can see a sharp peak at $\omega = 0$ produced by the localized state at the edge. This peak vanishes when we move towards the center of the ribbon as shown in panel (b) leading the system into a pure metallic region. Also in panels (b) and (c) the total DOS, averaged over all sites of the unit cell, is shown with red-dashed lines.

If we now couple a magnetic adatom to any of these systems, the behavior of the spin correlations will be determined by the electronic properties of the specific ribbon, and the position of the impurity.

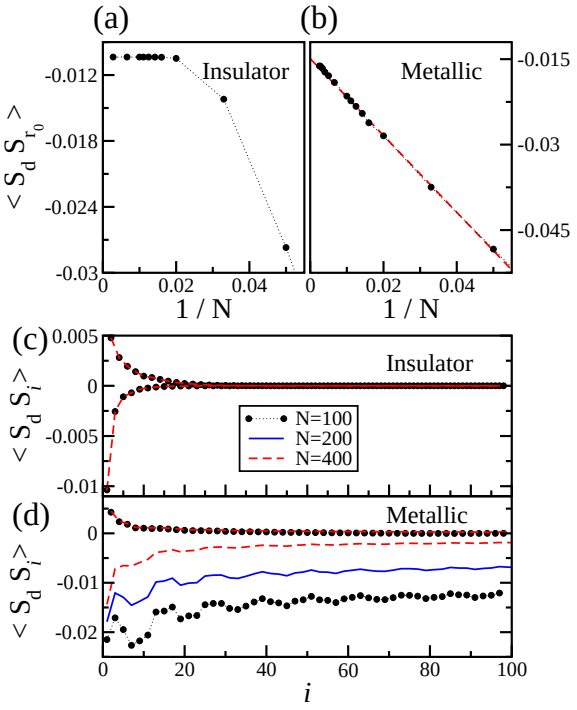

FIG. 11: *Correlations for an adatom in a armchair nanoribbon.* Panels (a) and (b) show the spin correlations between the impurity and the first site of the chain as a function of the inverse of the system size for an insulator ($n = 12$) and metallic ($n = 10$) nanoribbons. For the insulating case the correlations saturate, while in the metallic case the correlations scale linearly in $1/N$ (extrapolated curve is shown with red-dashed lines). In panels (c) and (d) the spin correlations between the impurity and the Lanczos orbitals are shown. Even and odd sites along the chain represent orbitals in different sublattices of the original problem.

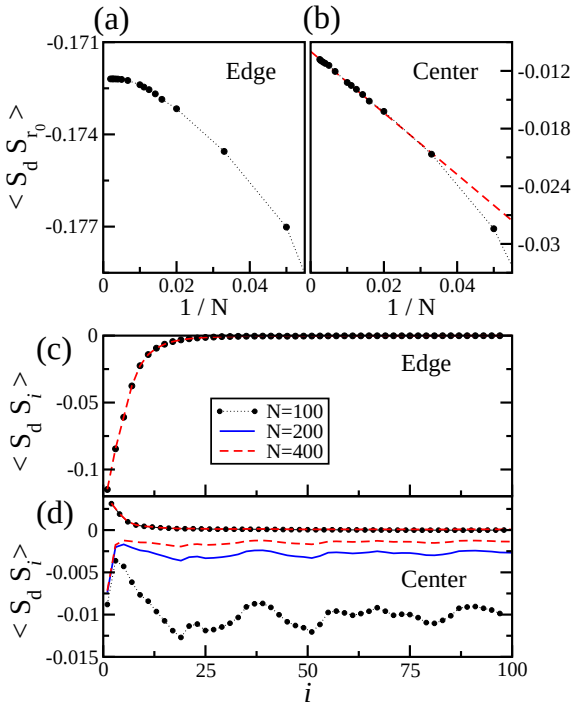

FIG. 12: *Correlations for an adatom in a zigzag nanoribbon.* Panel (a) and (b) present the spin correlations between the impurity and the first site of the Lanczos chain as a function of $1/N$. As mentioned in the text, the edge states are localized, and the correlations in (a) saturate. In (b) the impurity is at the center, and the bulk states are metallic. The correlations between the adatom as a function of the distance along the chain are presented in panels (c) for the impurity at the edge, and (d) for the impurity at the center.

B. Results for armchair ribbons

We first study the spin correlations for an adatom in a armchair ribbon. As in Sec. VI we use the impurity Anderson model (IAM) to describe the problem. The total Hamiltonian is given by Eqs. 1, 3 and 2. Unless otherwise stated, we work in the particle-symmetric point for $U = 0.5t$ and $V_g = -U/2$ and an hybridization $t' = \sqrt{0.05}$.

In Figure 11 we present results for a single Anderson impurity attached to insulating ($n = 12$) and metallic ($n = 10$) armchair ribbons. In both cases, we place the impurity at the center of the ribbon. Panel (a) and (b) shows the spin-spin correlations between the impurity and the first site of the chain, which is also the site of the real lattice attached to the impurity. For the insulating armchair ribbon, shown in panel (a), we can observe a saturation of the correlations occurring at systems sizes larger than $N = 50$ sites, which give an indication of the correlation length in the system.

Panels (c) and (d) show the spin correlations between the impurity and the sites of the mapped chain for the insulating and metallic ribbon respectively. In both cases we observe different behavior for the correlations corresponding to two different sublattices. Since the Lanczos method consists in successively applying the lattice Hamiltonian, each site of the mapped chain is associated to an specific sublattice of the real system. In this case odd sites of the Lanczos chain correspond to the same sublattice as the site connected to the impurity.

In panel (c) we again observe a fast convergence of the correlations with the system size. This correlations decay virtually to zero at distances of the order of 50 sites from the impurity, in agreement with the previous observation.

In the metallic case, shown in panel (d), the ferromagnetic correlations decay fast as in the previous case. However, the correlations within the same sublattice present a very slow decay. These correlations in the real space are associated with the size of the Kondo cloud, which is of the order of $1/T_K$,[6]. The decay of the correlations is very slow.

We also performed calculation with the impurity attached at the edge of the ribbon, esentially reproducing the same behavior.

C. Results for zigzag ribbons

We proceed in the same way to analyze the case of the zigzag ribbons, for the same model and parameters as in the previous section. This time we need to differentiate the edge from the bulk states of the ribbon. We studied a system with

an $n = 24$ unit cell, placing the impurity at the edge, and at the center.

Results are shown in Fig. 12. In panels (a) and (b), we show the extrapolation to the thermodynamic limit for the spin correlation between the impurity and the first site of the chain. For the case of the impurity attached to the edge of the zigzag ribbon, panel (a), we observe saturation at $N \sim 100$. When the impurity is attached to the center of the ribbon, shown in panel (b), the correlations scale linearly in $1/N$, as in the metallic case.

Panels (c) and (d) show the spin-spin correlations between the impurity and the Lanczos orbitals of the chain, as a function of the distance from the impurity. The results for the impurity at the center are shown in (d), showing similar behavior as the metallic armchair ribbon. Remarkably, the correlations do not display a noticeable decay in the observed range.

VIII. CONCLUSIONS

In this work we propose a canonical transformation based in the Lanczos method to map complex single particle band structures onto equivalent 1d systems. For the case of single impurities, this transformation preserves the form of the coupling Hamiltonian between the impurity and the lattice. The resulting many-body problem can be solved numerically with appropriate methods, such as DMRG, ECA, or QMC.

We have shown that complex systems like CNT with insulating gaps or Van Hove singularities can be perfectly represented and treated with this method. Using DMRG, we are able to study fairly large systems. As a benchmark and illustration, we showed that large d-dimensional systems can be studied with little effort, once their band structure is mapped onto the effective 1d Hamiltonian.

In addition, we studied adatoms in carbon nanotubes, and graphene nanoribbons. The complex and rich electronic properties of these systems, as well as their geometry, make them specially suitable for our method. We can clearly distinguish between insulating and metallic regimes, or edge and bulk states, depending on the geometry of the system, and the position of the impurity.

It is important to point out that extrapolations to the thermodynamic limit cannot be taken trivially in impurity problems. When the system is insulating, correlations decay exponentially, and we can easily obtain thermodynamic results. However, when the system is gapless, we need to recall that we are working in a Kondo box, where the inter-level spacing of the discrete band structure introduces an additional energy scale into the problem. Even though the short distance behavior can be obtained fairly accurately, we are far from the universal Kondo regime. This regime can only be reached with NRG, a method that is precisely designed to study this limit.

Possible of applications of the method include topological insulators, where the bulk and the boundary have very different electronic properties.

Even though we have used the DMRG to solve the effective one-dimensional problem, one could use alternative methods, such as ECA, or QMC, since the Hamiltonian has no sign problem. One could also use these methods to study time-dependent[74], and thermodynamic properties[75], as well as spectral functions[76,77].

In principle, any quadratic Hamiltonian can be mapped onto an equivalent 1d system following our prescription. This opens the doors to problems with spin-orbit interaction, and superconductors (at the mean field/BdG level).

The method can also become a powerful tool to study quantum chemistry problems in which a magnetic atom is embedded into a system that could be described by a Hückel-like theory. Moreover, one could use it in conjunction with ab-initio band structure calculations, incorporating the information about the bulk system into the effective 1d chain, and the hybridization terms in the structure of the seed state, paving the way toward realistic first principles modeling and understanding of correlation effects in quantum impurity problems.

Acknowledgments - We thank K. Al-Hassanieh and F. Heidrich Meisner for helpful discussions. C.A.B. was supported by the *Deutsche Forschungsgemeinschaft* (DFG) through FOR 912 under grant-no. HE5242/2-2. AEF acknowledges NSF support through grant DMR-1339564.

* Electronic address: carlos.busser@gmail.com

1. A. Hewson, *The Kondo Problem to Heavy Fermions* (Cambridge Univ. Press, 1997).
2. D. Cox and A. Zawadowski, Advances in Physics **47**, 599 (1998).
3. I. Affleck, arXiv preprint arXiv:0911.2209 (2009).
4. A. Holzner, I. P. McCulloch, U. Schollwöck, J. von Delft, and F. Heidrich-Meisner, Phys. Rev. B **80**, 205114 (2009).
5. G. Bergmann, Phys. Rev. B **77**, 104401 (2008).
6. C. A. Büsser, G. B. Martins, L. C. Ribeiro, E. V. A. E. Vernek, and E. Dagotto, Phys. Rev. B **81**, 045111 (2010).
7. P. Simon and I. Affleck, Phys. Rev. Lett. **89**, 206602 (2002).
8. P. Simon and I. Affleck, Phys. Rev. B **68**, 115304 (2003).
9. R. K. Kaul, G. Zaránd, S. Chandrasekharan, D. Ullmo, and H. U. Baranger, Phys. Rev. Lett. **96**, 176802 (2006).
10. T. Hand, J. Kroha, and H. Monien, Phys. Rev. Lett. **97**, 136604 (2006).
11. P. Schlottmann, Phys. Rev. B **65**, 024420 (2001).
12. K. G. Wilson, Rev. Mod. Phys. **47**, 773 (1975).
13. N. Andrei, K. Furuya, and J. Lowenstein, Rev. Mod. Phys. **55**, 331 (1983).
14. A. Tsvelik and P. Wiegmann, J. Phys. C:Solid State Phys. **16**, 2281 (1983).
15. R. Bulla, T. A. Costi, and T. Pruschke, Rev. Mod. Phys. **80**, 395 (2008).
16. L. Fritz and M. Vojta, Rep. Prog. Phys. **76**, 032501 (2013).
17. B. Uchoa, V. N. Kotov, N. Peres, and A. Castro Neto, Phys. Rev. Lett. **101**, 026805 (2008).
18. B. Uchoa, T. Rappoport, and A. Castro Neto, Physical Review Letters **106**, 016801 (2011).
19. T. Wehling, A. Balatsky, M. Katsnelson, A. Lichtenstein, and A. Rosch, Phys. Rev. B **81**, 115427 (2010).
20. T. Wehling, H. Dahal, A. Lichtenstein, M. Katsnelson,

H. Manoharan, and A. Balatsky, Phys. Rev. B **81**, 085413 (2010).
[21] R. Bulla, T. Pruschke, and A. Hewson, J. of Phys.: Condensed Matter **9**, 10463 (1997).
[22] M. F. Crommie, C. P. Lutz, and D. M. Eigler, Nature **363**, 524 (1993).
[23] V. Madhavan, W. Chen, T. Jamneala, M. F. Crommie, and N. S. Wingreen, Science **280**, 567 (1998).
[24] H. C. Manoharan, C. P. Lutz, and D. M. Eigler, Nature **403**, 512 (2000).
[25] T. Jamneala, V. Madhavan, and M. F. Crommie, Phys. Rev. Lett. **87**, 256804 (2001).
[26] M. Ternes, A. J. Heinrich, and W.-D. Schneider, J. Phys.: Condens. Matter **21**, 053001 (2009).
[27] N. Néel, J. Kröger, R. Berndt, T. Wehling, A. Lichtenstein, and M. Katsnelson, Phys. Rev. Lett. **101**, 266803 (2008).
[28] B. Uchoa, L. Yang, S.-W. Tsai, N. Peres, and A. Castro Neto, Phys. Rev. Lett. **103**, 206804 (2009).
[29] H. Prüser, M. Wenderoth, P. E. Dargel, A. Weismann, R. Peters, T. Pruschke, and R. G. Ulbrich, Nature Physics **7**, 203 (2011).
[30] J. Hirsch and R. Fye, Phys. Rev. Lett. **56**, 2521 (1986).
[31] J. Gubernatis, J. Hirsch, and D. Scalapino, Phys. Rev. B **35**, 8478 (1987).
[32] P. Werner, A. Comanac, L. DeMedici, M. Troyer, and A. J. Millis, Phys. Rev. Lett. **97**, 076405 (2006).
[33] E. Gull, P. Werner, O. Parcollet, and M. Troyer, EPL **82**, 57003 (2008).
[34] E. Gull, A. J. Millis, A. I. Lichtenstein, A. N. Rubtsov, M. Troyer, and P. Werner, Rev. Mod. Phys. **83**, 349 (2011).
[35] L. Borda, Phys. Rev. B **75**, 041307 (2007).
[36] I. Affleck, L. Borda, and H. Saleur, Phys. Rev. B **77**, 180404 (2008).
[37] A. K. Mitchell, M. Becker, and R. Bulla, Phys. Rev. B **84**, 115120 (2011).
[38] C. Gonzalez-Buxton and K. Ingersent, Phys. Rev. B **57**, 14254 (1998).
[39] R. Žitko, Computer Physics Communications **180**, 1271 (2009).
[40] S. R. White, Phys. Rev. Lett. **69**, 2863 (1992).
[41] S. R. White, Phys. Rev. B **48**, 10345 (1993).
[42] S. R. White and R. Noack, Phys. Rev. Lett. **68**, 3487 (1992).
[43] U. Schollwöck, Rev. Mod. Phys. **77**, 259 (2005).
[44] D. J. García, K. Hallberg, and M. J. Rozenberg, Phys. Rev. Lett. **93**, 246403 (2004).
[45] E. Dagotto, Rev. Mod. Phys. **66**, 763 (1994).
[46] P. Calabrese and J. Cardy, J. Stat. Mech.: Theory Exp. p. P06002 (2004).
[47] P. Calabrese and J. Cardy, Int. J. Quantum Inf. **4**, 429 (2006).
[48] M. M. Wolf, Phys. Rev. Lett. **96**, 010404 (2006).
[49] D. Gioev and I. Klich, Phys. Rev Lett. **96**, 100503 (2006).
[50] W. Li, L. Ding, R. Yu, T. Roscilde, and S. Haas, Phys. Rev. B **74**, 073103 (2006).
[51] T. Barthel, M.-C. Chung, and U. Schollwöck, Phys. Rev. A **74**, 022329 (2006).
[52] A. Feiguin and C. Büsser, Phys. Rev. B **84**, 115403 (2011).
[53] G. D. R. Saito, M. S. Dresselhaus, *Physical Properties of Carbon Nanotubes* (World Scientific, 1998).
[54] K. S. Novoselov, A. K. Geim, S. V. Morozov, D. Jiang, Y. Zhang, S. V. Dubonos, I. V. Grigorieva, and A. A. Firsov, Science **306**, 666 (2004).
[55] K. S. Novoselov, A. K. Geim, S. V. Morozov, D. Jiang, M. I. Katsnelson, I. V. Grigorieva, S. V. Dubonos, and A. A. Firsov, Nature **438**, 197 (2005).
[56] A. H. Castro-Neto, F. Guinea, N. M. R. Peres, K. S. Novoselov, and A. K. Geim., Rev. Mod. Phys. **81**, 109 (2009).
[57] S. D. Sarma, S. Adam, E. H. Hwang, , and E. Rossi, Rev. Mod. Phys. **83**, 407 (2011).
[58] C. Berger, Z. Song, X. li, X. Wu., N. Brown, C. Naud, D. Mayou, T. Li, J. Haas, and A. Marchenkov, Science **312**, 1191 (2006).
[59] P. Avouris, Z. Chen, and V. Perebeinos, Nature Nanotech. **2**, 605 (2007).
[60] A. K. Geim and K. S. Novoselov, Nature. Mater. **6**, 183 (2007).
[61] Y.-M. Lin, K. A. Jenkins, A. Valdes-García, J. Small, D. B. Farmer, and P. Avouris, Nano Lett. **9**, 4474 (2009).
[62] S. A. Wolf, D. D. Awschalom, R. A. Buhrman, J. M. Daughton, S. von Volnar, M. Roukes, A. Y. Chtchelkanova, and D. M. Treger, Science **294**, 1488 (2001).
[63] I. Zutić, J. Fabiana, and S. D. Sarma, Rev. Mod. Phys. **76**, 323 (2004).
[64] A. Castro Neto, V. N. Kotov, J. Nilsson, V. M. Pereira, N. M. Peres, and B. Uchoa, Solid State Communications **149**, 1094 (2009).
[65] A. V. Shytov, D. A. Abanin, and L. S. Levitov, Phys. Rev. Lett. **103**, 016806 (2009).
[66] J.-H. Chen, L. Li, W. G. Cullen, E. D. Williams, and M. S. Fuhrer, Nature Physics **7**, 535 (2011).
[67] P. S. Cornaglia, G. Usaj, and C. Balseiro, Phys. Rev. Lett. **102**, 046801 (2009).
[68] K. Sengupta and G. Baskaran, Phys. Rev. B **77**, 045417 (2008).
[69] D. Jacob and G. Kotliar, Phys. Rev. B **82**, 085423 (2010).
[70] T. O. Wehling, A. V. Balatsky, M. I. Katsnelson, A. I. Lichtenstein, and A. Rosch., Phys. Rev. B **81**, 115427 (2010).
[71] M. Kharitonov and G. Kotliar, arXiv preprint arXiv:1305.0075 (2013).
[72] I. Schneider, L. Fritz, F. Anders, A. Benlagra, and M. Vojta, Phys. Rev. B **84**, 125139 (2011).
[73] K. Nakada, M. Fujita, G. Dresselhaus, and M. Dresselhaus, Phys. Rev. B **54**, 17954 (1996).
[74] S. R. White and A. E. Feiguin, Phys. Rev. Lett. **93**, 076401 (2004).
[75] A. E. Feiguin and S. R. White, Phys. Rev. B **72**, 220401(R) (2005).
[76] T. Barthel, U. Schollwöck, and S. R. White, Phys. Rev. B **79**, 245101 (2009).
[77] A. E. Feiguin and G. A. Fiete, Phys. Rev. B **81**, 075108 (2010).